Quantum Electronics **50** (6) 520–524 (2020)

https://doi.org/10.1070/QEL17362

Trapping of lithium atoms in a large hollow optical dipole trap

V.A. Vinogradov, K.A. Karpov, S.S. Lukashov, A.V. Turlapov

Abstract. **We describe the trapping of lithium atoms in an optical dipole trap about 1 mm in size, with a nearly rectangular potential. The trap has the shape of a cylinder with flat bases. The confinement region is bounded by thin walls produced by light with a frequency blue-detuned from an atomic transition (resonance) frequency by 19 GHz. Before trapping, the gas is collected and cooled in a magneto-optical trap whose centre nearly coincides with the centre of the dipole trap. After switching off the magneto-optical trap, we have photographed the atoms remaining in the dipole trap.**

Keywords: *laser trapping and cooling, gas of atoms, dipole force.*

1. Introduction

The laser cooling and trapping of atoms [1–3] has found wide application in basic and applied research. There are frequency and time standards based on ultracold atomic gases [4, 5]. The interference of de Broglie waves of atoms allows angular and linear accelerations to be measured with high accuracy [6]. A gas of ultracold atoms excited to Rydberg states [7–9] is a promising medium for implementing quantum information algorithms [10]. In experiments with ultracold gases of bosonic and fermionic atoms, a number of effects were observed for the first time, whose mathematical models are basic to quantum physics, e. g. Fermi pressure [11] and Bose–Einstein condensation [12]. Bose condensates [13–19] and Fermi gases of atoms [13, 20, 21] are the subject of intense research. Increasing the number of trapped atoms is of interest owing to effects proportional to $N^2, N, N^{-1/2}$ and $N^{-1/3}$, where a small exponent does not downplay the importance of the effect. N^2 behaviour corresponds to coherent light effects. Thermodynamic quantities are proportional to N. $N^{-1/2}$ behaviour is characteristic of shot noise in measurements, and $N^{-1/3}$ behaviour is encountered in many-body problems. For example, the fraction of surface atoms in a cubic cloud is $6N^{-1/3}$, which allows one to estimate the contribution of surface effects. Thus, increasing N is important for simulating bulk properties of solids using an atomic gas in an optical lattice [13, 22].

The lowest attainable temperature of atoms in a trap, expressed as a dimensionless quantity, also depends on N. Its natural dimensionless scale is the chemical potential μ. In a closed system, the lowest observed temperature corresponds to the excitation of a single particle or quasiparticle to above the level of the chemical potential. Thus, $T_{\min}$ can be estimated as the energy separation between two single-particle states near μ. In a rectangular potential well, we have $T_{\min}/\mu = 2N^{-1/3}$ for an ideal Fermi gas and $T_{\min}/\mu \sim N^{-7/15}$ for a weakly interacting Bose gas. It is the dimensionless temperature which is important for phase transitions and, hence, in search of new transitions it is important to increase N.

The largest N in a highly degenerate Fermi gas was obtained for ^{6}Li atoms: 10^7 at $T_{\min}/\mu = 0.1$ [23]. The largest Bose–Einstein condensate contains $N = 10^8$ sodium atoms [24]. The lowest temperature in absolute units, 450 pK, was reached in a Bose–Einstein condensate of $N = 2500$ particles [25], which corresponds to 0.7 of the Bose condensation temperature and considerably exceeds μ = 33 pK. Thus, the number of particles in quantum gases is noticeably smaller than that in problems of superfluidity of helium [26, 27] and superconductivity [28, 29]. An increase in N is possible because, in a precooling step in a magneto-optical trap (MOT), the number of atoms is $\sim 10^{10}$ [24, 30].

A large hollow optical dipole trap, capable of accepting all particles from an MOT, allows one, in principle, to prepare a quantum gas with a significant fraction of atoms retained [31]. For example, in the case of evaporative cooling, beginning from a phase density characteristic of MOTs one can reach quantum degeneracy with one-third of the particles retained [32]. Hollow traps with a quasi-uniform potential in them are also of interest in search of novel phenomena. In the case of partially spin-polarised Fermi gases, they open up the possibility of observing Fulde–Ferell–Larkin–Ovchinnikov superfluidity [33, 34] and pairing in the p-wave channel by the Kohn–Luttinger mechanism [35–37]. These effects have not been detected in a parabolic trap because, most likely, they are outplayed by phase separation into a completely paired and a completely spin-polarised gas. Moreover, uniformity of the potential removes limitations on correlation radii near phase transitions. In parabolic traps, such limitations arise from the nonuniform concentration of atoms.

In a previous study, Kuga et al. [38] demonstrated an optical dipole trap more than 1 mm in size for rubidium atoms. The trap had thick and slightly inclined walls, whose volume was of the order of the trap volume. Later, traps were reported with thin walls and, accordingly, a more uniform confinement region. Those traps were used to prepare uniform Bose [39] and Fermi [40–42] gases. The traps were ~100 μm in size.

In this paper, we report an optical dipole trap ~1 mm in size with an almost rectangular potential and the use of the trap for confining lithium-6 atoms precooled in a magneto-optical trap.

V.A. Vinogradov, K.A. Karpov, S.S. Lukashov, A.V. Turlapov Institute of Applied Physics (Federal Research Centre), Russian Academy of Sciences, ul. Ulyanova 46, 603950 Nizhny Novgorod, Russia; e-mail: turlapov@appl.sci-nnov.ru

Received 11 March 2020; revision received 6 April 2020
Kvantovaya Elektronika **50** (6) 520–524 (2020)
Translated by O.M. Tsarev

2. Experimental

The optical fields producing the dipole trap are schematised in Fig. 1a. The vertical tube with a circular cross section limits the motion of atoms in the xy plane, and their motion along the z axis is limited by flat walls. A laser beam in the form of a tube was obtained using the configuration schematised in Fig. 2. We chose a configuration with the smallest possible number of optical components, which helped minimise field distribution nonuniformities. In Fig. 2, the window of the vacuum chamber and the polarising cube on which the ring-shaped light beam is aligned with a vertical beam of an MOT are omitted. The optical fields produce a repulsive dipole potential, because the laser frequency ω exceeds the frequency ω_0 of the nearest electric dipole transition in atoms. The dipole force potential $U(\boldsymbol{r})$ is related to the light intensity $I(\boldsymbol{r})$ profile as follows [43]:

$$U(\boldsymbol{r}) = \frac{3\pi c^2 \Gamma I(\boldsymbol{r})}{2\omega_0^3(\omega - \omega_0)}, \qquad (1)$$

where Γ is the inverse of the excited state lifetime of the atom. It is seen from (1) that a small $\omega - \omega_0$ detuning allows a high potential to be generated around a trap with a large volume. A dipole trap for ^{6}Li atoms is produced by light with a frequency blue-detuned by $(\omega - \omega_0)/2\pi = 19 \pm 3$ GHz relative to the frequency of the D_2 line of the $2S_{1/2} \rightarrow 2P_{3/2}$ transition at a wavelength of 671 nm. The power of the ring-shaped beam is 120 mW, the half-intensity thickness of the ring walls in the smallest thickness plane is 34 μm, and the ring diameter is 1.0 mm, which corresponds to a potential of 360 K. The flat walls are formed by light beams, each of 45 mW power. Their elliptical profile has half-intensity dimensions of 45 μm and 1.7 mm, producing 190-μK-high barriers.

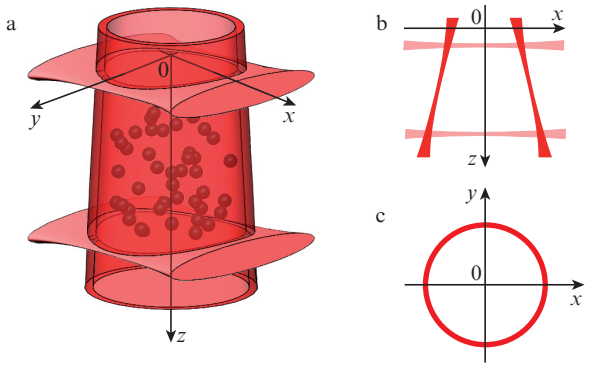

Figure 1. (Colour online) Trapping of gas atoms (shown as circles) in a region bounded by light beams (shown red) (a) and the xz (b) and xy (c) sections of the beams.

Each experiment begins with the preparation of a cloud of lithium-6 atoms in an MOT, which is loaded from a beam of atoms slowed down to ~30 m s^{-1} with the use of a Zeeman slower [44, 45]. The magnetic field of the MOT is axisymmetric in the vertical direction (z), with a vertical gradient of 30 G cm^{-1}. The MOT is produced using light with $\lambda = 671$ nm, near the D_2 line. The preparation of the atomic cloud in the MOT comprises two stages, differing in time: accumulation and final cooling. In the accumulation stage, which lasts 20 s, each of the six trapping beams has a power of 30 mW and an intensity of 25 mW cm^{-2} at its centre. Each beam comprises components at two frequencies. In the vertical beams, 70% of the power is accounted for by a frequency 5Γ below the frequency of the $2S_{1/2}(F = 3/2) \rightarrow 2P_{3/2}$ transition, and the rest of the light (30%) has the same frequency detuning from the $2S_{1/2}(F = 1/2) \rightarrow 2P_{3/2}$ transition. In the horizontal beams, the ratio is 90 : 10. Figure 3 shows an image of a cloud obtained after 20 s of accumulation (the imaging method is described below). The temperature of the atoms in the MOT, as evaluated from the expansion of the cloud after the MOT beams are switched off, is 3–4 mK. To lower the temperature [45], the accumulation stage is followed by the final cooling stage, which lasts 0.5 ms. During this stage, the detuning of the optical fields of the MOT is just 0.5Γ and the power is reduced by 70 times. After it, the optical fields of the MOT are switched off.

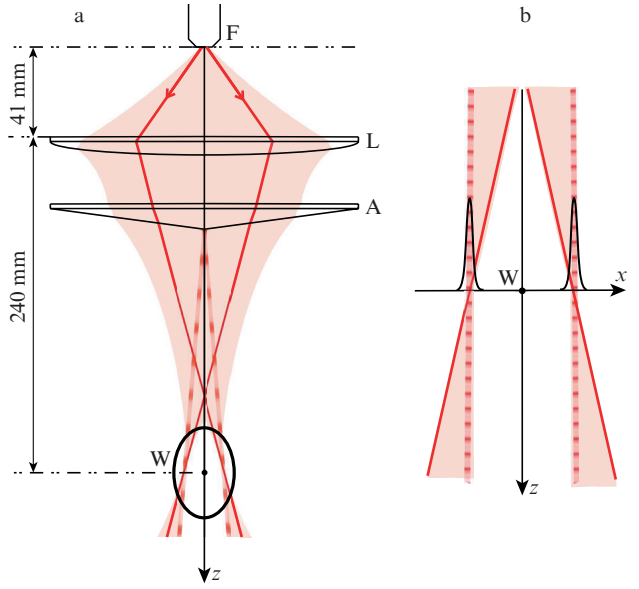

Figure 2. (Colour online) (a) Optical configuration for producing a ring-shaped light beam from a beam with a Gaussian transverse mode and (b) enlarged view of the ring-shaped beam region:
F, optical fibre acting as a transverse mode source (total beam divergence angle, 10.1°); L, lens with a focal length of 35 mm; A, axicon with a base angle of 0.5°, placed almost next to the lens; W, beam waist region (where the beam takes the shape of a tube). The red lines and shading represent ray trajectories in the geometrical optics approximation, the dashed lines show trajectories of the rays issuing from the centre of the axicon; and the solid lines show the calculated intensity distribution in the focal plane.

The relative positions of the atomic cloud in the MOT and the dipole trap beams are shown in Fig. 4, which presents a photograph of fluorescence of atoms located simultaneously in the fields of the MOT and dipole trap beams. To visualise the image, the emission frequency of the dipole trap is tuned not to the trapping frequency ω but to the resonance frequency of the $2S_{1/2}(F = 1/2) \rightarrow 2P_{3/2}$ transition, the magnetic field gradient is under 30 G cm^{-1}, the dipole trap beam power is of the order of 1 mW, and the MOT filling time is increased, which leads to an increase in cloud size.

The optical dipole trap is turned on 10 ms before switching off the MOT beams, which is performed in two steps. First, the light at the frequency depleting the $2S_{1/2}(F = 1/2)$ level is turned off. Next, after 150 μs the light close in frequency to the $2S_{1/2}(F = 3/2) \rightarrow 2P_{3/2}$ transition is turned off. This sequence leads to an increase in the population of the

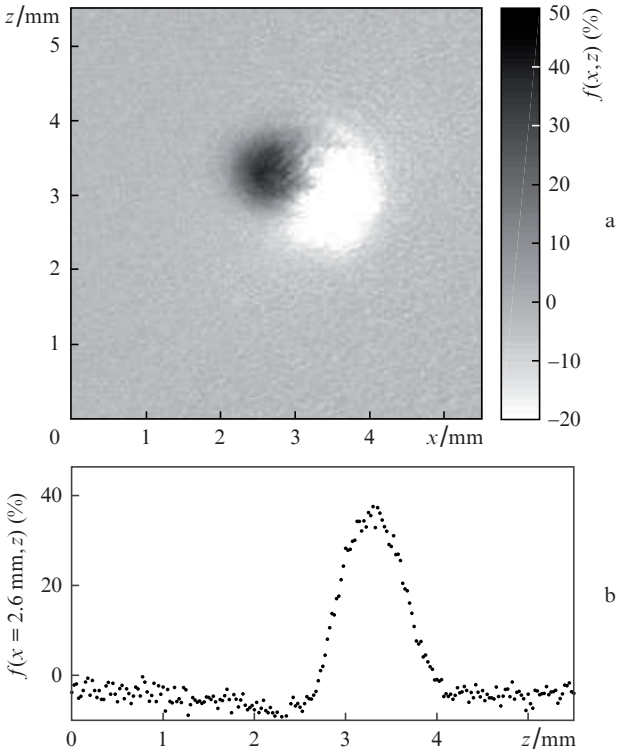

Figure 3. Resonant absorption image of the atomic cloud after the 20-s accumulation stage (immediately after the MOT beams are switched off) in the absence of the dipole trap: (a) $f(x, y)$ is the fraction of the light absorbed in the plane of the object; the dark spot is the shadow of the cloud; and the light spot is due to the fluorescence of the cloud in the MOT field, which leads to apparent negative absorption (unwanted effect); (b) profile along the z axis through the centre of the cloud: $f(x = 2.6\ \text{mm}, z)$.

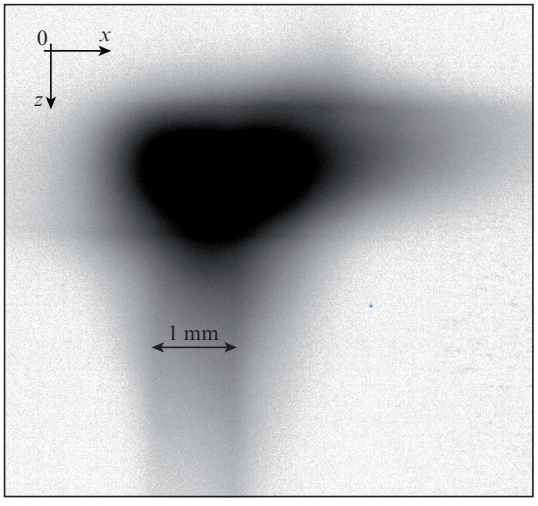

Figure 4. Photograph of fluorescence of atoms in the field of the MOT beams and three dipole trap beams. The spatial scale can be estimated from the thickness of the vertical ring-shaped beam: 1 mm.

$2S_{1/2}(F = 1/2)$ level. The magnetic field gradient is maintained throughout the experiment. After switching off the MOT beams, the atoms are only confined by the optical dipole trap, whereas the trapping by the remaining quadrupole magnetic field of the MOT can be neglected.

Atomic gas can be imaged using light absorption [44, 45]. Figure 3a presents an image of the cloud after the accumulation stage in the MOT, immediately after switching off the optical fields of the MOT, with no final cooling stage and no dipole trap, and Fig. 5a presents an image of the gas in the optical dipole trap. To obtain the image, the gas is illuminated with a light pulse at the resonance frequency of the $2S_{1/2}(F = 1/2) \rightarrow 2P_{3/2}$ transition. The emission intensity is 0.013 mW cm^{-2} and the pulse duration is 60 μs for the image in Fig. 3a and 80 μs for the image in Fig. 5a. The shadow of the cloud is projected onto the CCD array. Figures 3 and 5 present spatial distributions of light absorption by the cloud, $f(x, z)$, calculated in the plane of the imaging subject as the ratio of the scattered light intensity to the intensity of illumination light propagating in the y direction.

The image in Fig. 5a was obtained 1 ms after completely switching off the MOT beams and presents a side view of a cylindrical dipole trap. In the central part of the image, an atomic cloud is seen, which has sharp boundaries and a nearly rectangular projection onto the xz plane. Figures 5b and 5c present results of averaging the image along the z and x axes:

$$f_{1x}(x) = \frac{1}{z_2 - z_1}\int_{z_1}^{z_2} f(x,z)\,\mathrm{d}z,$$

$$f_{1z}(z) = \frac{1}{x_2 - x_1}\int_{x_1}^{x_2} f(x,z)\,\mathrm{d}x, \qquad (2)$$

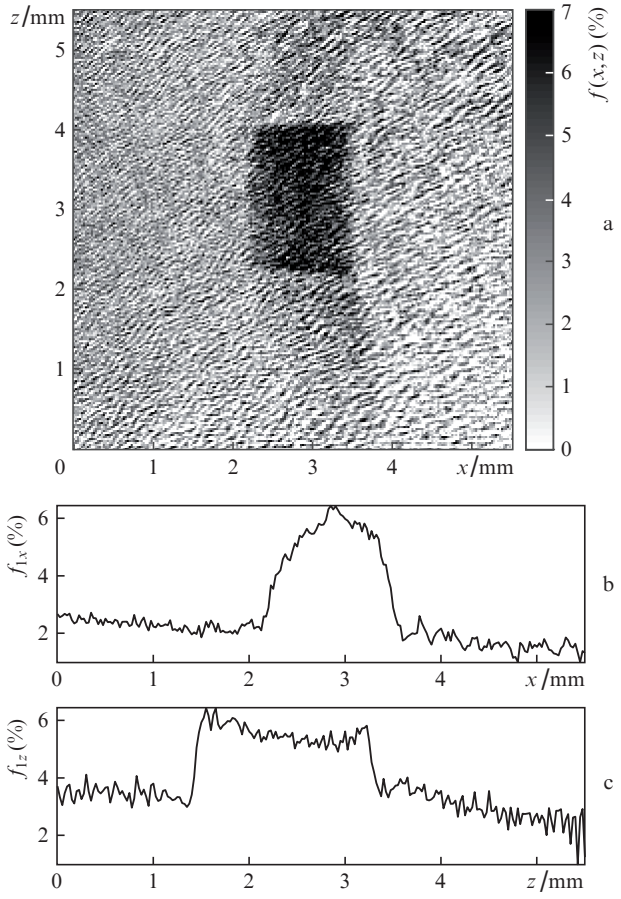

Figure 5. Spatial distribution of light absorption by the cloud of trapped atoms 1 ms after switching off the MOT (a) and results of integrating the image along the z (b) and x (c) axes.

where x_1, x_2, z_1 and z_2 are the coordinates of the trap boundaries. The z-axis profile has the form of a plateau, whereas the x-axis profile has a rounded shape. The absorption profiles correspond to an almost uniform filling of the cylindrical trap with atoms and indicate that their motion is restricted by the trap walls, i.e. they are trapped.

To confirm the trapping, consider possible dynamics of the cloud after switching off the MOT in the absence of the dipole trap. To estimate the initial shape and size of the cloud, we can use the data in Fig. 3, where the concentration profile is almost Gaussian and the rms radius of the cloud is 0.26 mm along the x axis and 0.28 mm along the z axis. We neglect the fact that the radius can be slightly larger because of the cloud expansion in the final cooling stage. The atom temperature after the final cooling stage in the MOT was not measured. Its upper limit is the temperature in the trap filling step, 3–4 mK, which corresponds to an atom velocity $\sqrt{T/m} = 2.0–2.4$ m s^{-1} (where m is the atomic mass). In the final cooling stage, the temperature can be 0.7 mK [45]. Note that it cannot be below the Doppler limit $\hbar\Gamma/2 = 0.15$ K [46], which corresponds to an atom velocity of 0.5 m s^{-1}. Temperatures in the range 0.15–4 mK mean that, after expansion for 1 ms, the cloud will have a Gaussian spherically symmetric concentration profile with an rms radius from 0.5 to 2.4 mm, which differs qualitatively from the profile in Fig. 5. The trapping can only be accounted for by the potential part of the dipole force. The viscous part of the dipole force is insignificant because its frequency detuning is too large for cooling purposes and the dipole trap is formed by travelling waves.

In Fig. 5, unconfined atoms are seen in the tube above and below the cloud. These can be not only the atoms that were initially outside the dipole trap but also those lost from it. The number of trapped atoms, N, can be estimated from the image in Fig. 5a by relating the fraction of the light absorbed, f, to the concentration n distribution in the two-level atom approximation:

$$\ln(1 - f(x,z)) = -\sigma \int n(x,y,z)\,\mathrm{d}y, \tag{3}$$

where $\sigma = \lambda^2/\pi$ is the illumination light scattering cross section averaged over possible transitions. As a result, we obtain $N = 6 \times 10^5$. Each atom scatters five photons during the imaging time (80 μs). Therefore, some of the atoms are pumped to the $2S_{1/2}(F = 3/2)$ state and stop scattering. Thus, the above value of N is the lower estimate. Similarly, for Fig. 3 we find $N = 1.3 \times 10^6$.

3. Discussion

To quantitatively evaluate light absorption data and determine N, a number of difficulties should be overcome. First, the numbers of atoms measured by two different methods differ by two orders of magnitude. From the images in Figs 3a and 5a, we obtain $N \sim 10^6$. At the same time, the fluorescence intensity of the atoms in the MOT, detected by a photomultiplier at the end of the accumulation stage, corresponds to $\sim 10^8$ atoms. Second, the horizontal cloud size seen in Fig. 5, $x_2 - x_1 = 1.4$ mm, exceeds the diameter of the ring-shaped beam, 1.0 mm, determined by directly measuring the intensity distribution. The magnification of the optical system was calibrated by shifting the horizontal wall of the trap by a known distance and examining the corresponding shift of the cloud boundary in the image. The calibration uncertainty, ± 8 %, is insufficient for accounting for the large visible cloud size. Refraction of light by the cloud can distort its size. Unaccounted refraction is evidenced by the surges in the f_{1z} profile at the boundaries of the cloud. Third, Fig. 5 shows a nonzero visible absorption far away from the cloud, which can be seen in the one-dimensional distributions f_{1x} and f_{1z}.

The lifetime of atoms in the trap was not measured, nor was the main loss channel identified. It is reasonable to assume that, because of the small $\omega - \omega_0$ detuning, the main loss mechanism is heating due to Rayleigh scattering by atoms that are in contact with the walls. The increase in the energy of an atom per unit time can be evaluated as

$$\dot{E} = \frac{\hbar\omega^2\Gamma}{2mc^2}\,\frac{\alpha U_{\max}}{\omega - \omega_0}, \tag{4}$$

where $\alpha \approx 0.2$ is the ratio of the volume of the walls to the trap volume and $U_{\max}$ is the height of the potential [31]. Therefore, the lifetime of an atom in the trap is $U_{\max}/\dot{E} = 30$ ms. Such heating can, in principle, be compensated for by rapid cooling.

Cooling without loss of particles can be performed using optical molasses [38]. In the case of lithium-6, cooling to below the Letokhov–Minogin–Pavlik limit can be performed in optical molasses not on the D_2 line, which is used for MOTs, but on the D_1 line and leads to a decrease in temperature to 40 μK or below in ∼1 ms [47]. For subsequent evaporative cooling [32], a dynamic increase in $\omega - \omega_0$ detuning is necessary.

Thus, we have presented preliminary results on the trapping of a gas of lithium-6 atoms in an optical dipole trap about 1 mm in size. The confinement region is bounded by thin walls produced by light with a frequency blue-detuned from the resonance frequency by 19 GHz. The trap has the shape of a cylinder with flat bases. We observe trapping of atoms in the dipole trap 1 ms after switching off the MOT.

Acknowledgements. V.A. Vinogradov and K.A. Karpov acknowledge the support of the Russian Science Foundation (Grant No. 18-12-00002), S.S. Lukashov received support from the RF Ministry of Science and Higher Education (state research task, Theme No. 0035-2019-0002), and A.V. Turlapov acknowledges the support of the Russian Foundation for Basic Research (Project Nos. 18-42-520024, 19-02-00585 and 19-29-11025).

References

1. Balykin V.I., Minogin V.G., Letokhov V.S. *Rep. Prog. Phys.*, **63**, 1429 (2000).
2. Onofrio R. *Phys. Usp.*, **59**, 1129 (2016) [*Usp. Fiz. Nauk*, **186**, 1229 (2016)].
3. Ryabtsev I.I., Kolachevsky N.N., Taichenachev A.V. *Quantum Electron.*, **49**, 409 (2019) [*Kvantovaya Elektron.*, **49**, 409 (2019)].
4. Taichenachev A.V., Yudin V.I., Bagaev S.N. *Phys. Usp.*, **59**, 184 (2016) [*Usp. Fiz. Nauk*, **186**, 193 (2016)].
5. Khabarova K.Yu., Kalganova E.S., Kolachevsky N.N. *Phys. Usp.*, **61**, 203 (2018) [*Usp. Fiz. Nauk*, **188**, 221 (2018)].
6. Cronin A.D., Schmiedmayer J., Pritchard D.E. *Rev. Mod. Phys.*, **81**, 1051 (2009).
7. Lim J., Lee H., Ahn J. *J. Korean Phys. Soc.*, **63**, 867 (2013).
8. Zelener B.B., Arshinova I.D., Bobrov A.A., Vilshanskaya E.V., Saakyan S.A., Sautenkov V.A., Zelener B.V., Fortov V.E. *JETP Lett.*, **108**, 820 (2018) [*Pis'ma Zh. Eksp. Teor. Fiz.*, **108**, 829 (2018)].

9. Yakshina E.A., Tretyakov D.B., Entin V.M., Beterov I.I., Ryabtsev I.I. *JETP*, **130**, 170 (2020) [*Zh. Eksp. Teor. Fiz.*, **157**, 206 (2020)].
10. Ryabtsev I.I., Beterov I.I., Tretyakov D.B., Entin V.M., Yakshina E.A. *Phys. Usp.*, **59**, 196 (2016) [*Usp. Fiz. Nauk*, **186**, 206 (2016)].
11. Truscott A.G., Strecker K.E., McAlexander W.I., Partridge G.B., Hulet R.G. *Science*, **291**, 2570 (2001).
12. Anderson M.H., Ensher J.R., Matthews M.R., Wieman C.E., Cornell E.A. *Science*, **269**, 198 (1995).
13. Bloch I., Dalibard J., Zwerger W. *Rev. Mod. Phys.*, **80**, 885 (2008).
14. Stamper-Kurn D.M., Ueda M. *Rev. Mod. Phys.*, **85**, 1191 (2013).
15. Il'ichov L.V., Chapovsky P.L. *Quantum Electron.*, **47**, 463 (2017) [*Kvantovaya Elektron.*, **47**, 463 (2017)].
16. Ruban V.P. *JETP Lett.*, **108**, 605 (2018) [*Pis'ma Zh. Eksp. Teor. Fiz.*, **108**, 638 (2018)].
17. Dalfovo F., Bisset R.N., Mordini C., Lamporesi G., Ferrari G. *JETP*, **127**, 804 (2018) [*Zh. Eksp. Teor. Fiz.*, **154**, 949 (2018)].
18. Stringari S. *J. Exp. Theor. Phys.*, **127**, 844 (2018) [*Zh. Eksp. Teor. Fiz.*, **154**, 964 (2018)].
19. Porozova V.M., Pivovarov V.A., Gerasimov L.V., Kupriyanov D.V. *JETP Lett.*, **108**, 714 (2018) [*Pis'ma Zh. Eksp. Teor. Fiz.*, **108**, 726 (2018)].
20. Giorgini S., Pitaevskii L.P., Stringari S. *Rev. Mod. Phys.*, **80**, 1215 (2008).
21. Kagan M.Yu., Turlapov A.V. *Phys. Usp*., **62**, 215 (2019) [*Usp. Fiz. Nauk*, **189**, 225 (2019)].
22. Vishnyakova G.A., Golovizin A.A., Kalganova E.S., Sorokin V.N., Sukachev D.D., Tregubov D.O., Khabarova K.Yu., Kolachevsky N.N. *Phys. Usp.*, **59**, 168 (2016) [*Usp. Fiz. Nauk*, **186**, 176 (2016)].
23. Zwierlein M.W., Schunck C.H., Schirotzek A., Ketterle W. *Nature* (London), **442**, 54 (2006).
24. Van der Stam K.M.R., van Ooijen E.D., Meppelink R., Vogels J.M., van der Straten P. *Rev. Sci. Instrum.*, **78**, 013102 (2007).
25. Leanhardt A.E., Pasquini T.A., Saba M., Schirotzek A., Shin Y., Kielpinski D., Pritchard D.E., Ketterle W. *Science*, **301**, 1513 (2003).
26. Kagan M.Yu. *Phys. Usp.*, **37**, 69 (1994) [*Usp. Fiz. Nauk*, **164**, 77 (1994)].
27. Nemirovskii S.K. *Fiz. Nizk. Temp.* (Kiev), **45**, 986 (2019).
28. Kagan M.Yu., Klaptsov A.V., Brodskii I.V., Combescot R., Leyronas X. *Phys. Usp.*, **49**, 1079 (2006) [*Usp. Fiz. Nauk*, **176**, 1105 (2006)].
29. Kopaev Yu.V., Belyavskii V.I., Kapaev V.V. *Phys. Usp.*, **51**, 191 (2008) [*Usp. Fiz. Nauk*, **178**, 202 (2008)].
30. Ridinger A., Chaudhuri S., Salez T., Eismann U., Fernandes D.R., Magalhãaes K., Wilkowski D., Salomon C., Chevy F. *Eur. Phys. J. D*, **65**, 223 (2011).
31. Vinogradov V.A., Karpov K.A., Savelyeva S.V., Turlapov A.V. *Quantum Electron.*, **49**, 433 (2019) [*Kvantovaya Elektron.*, **49**, 433 (2019)].
32. Luo L., Clancy B., Joseph J., Kinast J., Turlapov A., Thomas J.E. *New J. Phys.*, **8**, 213 (2006).
33. Fulde P., Ferrell R.A. *Phys. Rev.*, **135**, A550 (1964).
34. Larkin A.I., Ovchinnikov Yu.N. *Sov. Phys. JETP*, **20**, 762 (1965) [*Zh. Eksp. Teor. Fiz.*, **47**, 1136 (1964)].
35. Kohn W., Luttinger J.M. *Phys. Rev. Lett.*, **15**, 524 (1965).
36. Fay D., Layzer A. *Phys. Rev. Lett.*, **20**, 187 (1968).
37. Kagan M.Yu., Chubukov A.V. *JETP Lett.*, **47**, 614 (1988) [*Pis'ma Zh. Eksp. Teor. Fiz.*, **47**, 525 (1988)].
38. Kuga T., Torii Y., Shiokawa N., Hirano T., Shimizu Y., Sasada H. *Phys. Rev. Lett.*, **78**, 4713 (1997).
39. Gaunt A.L., Schmidutz T.F., Gotlibovych I., Smith R.P., Hadzibabic Z. *Phys. Rev. Lett.*, **110**, 200406 (2013).
40. Mukherjee B., Yan Z., Patel P.B., Hadzibabic Z., Yefsah T., Struck J., Zwierlein M.W. *Phys. Rev. Lett.*, **118**, 123401 (2017).
41. Hueck K., Luick N., Sobirey L., Siegl J., Lompe T., Moritz H. *Phys. Rev. Lett.*, **120**, 060402 (2018).
42. Baird L., Wang X., Roof S., Thomas J.E. *Phys. Rev. Lett.*, **123**, 160402 (2019).
43. Grimm R., Weidemüller M., Ovchinnikov Y.B. *Adv. At. Mol. Opt. Phys.*, **42**, 95 (2000).
44. Martyanov K.A., Makhalov V.B., Turlapov A.V. *JETP Lett.*, **91**, 369 (2010) [*Pis'ma Zh. Eksp. Teor. Fiz.*, **91**, 401 (2010)].
45. Hulet R.G., Nguyen J.H.V., Senaratne R. *Rev. Sci. Instrum.*, **91**, 011101 (2020).
46. Letokhov V.S., Minogin V.G., Pavlik B.D. *Sov. Phys. JETP*, **45**, 698 (1977) [*Zh. Eksp. Teor. Fiz.*, **72**, 1328 (1977)].
47. Burchianti A., Valtolina G., Seman J.A., Pace E., De Pas M., Inguscio M., Zaccanti M., Roati G. *Phys. Rev. A*, **90**, 043408 (2014).